

## Article

# Optimal Design of Mix Proportion of Hot-Mix Epoxy Asphalt Mixture for Steel Bridge Decks and Its Anti-Slip Performance

Wen Nie <sup>1,2,\*</sup> , Duanyi Wang <sup>1</sup>, Junjian Yan <sup>2</sup> and Xiaoning Zhang <sup>1,2</sup>

<sup>1</sup> School of Civil Engineering and Transportation, South China University of Technology, Wushan Road, Tianhe District, Guangzhou 510641, China; tcdywang@scut.edu.cn (D.W.); ctxnzh@scut.edu.cn (X.Z.)

<sup>2</sup> Guangzhou Xiaoning Roadway Engineering Technology Research Institute Co., Ltd., Wushan Road, Tianhe District, Guangzhou 510641, China; junjianyan@outlook.com

\* Correspondence: 202010101505@mail.scut.edu.cn

**Abstract:** To solve the problem of the insufficient anti-slip performance of steel bridge deck wear layers, a kind of new epoxy asphalt mixture FAC-10 (Full Epoxy Asphalt Content is shortened to FAC) is proposed in this paper based on the design method of an asphalt-rich mix proportion. The FAC-10 pavement layer was tracked and tested using a pavement texture tester to study the change in its skid resistance under traffic load from a macroscopic and microscopic perspective. The influence of traffic load on the deformation of the FAC-10 wearing layer was also simulated and analyzed via lab tests. The results show that the new FAC-10 epoxy asphalt mixture is superior to the traditional EA-10 epoxy asphalt mixture in terms of skid resistance. During the monitoring and testing period, the three-dimensional (3D) structure depth of the pavement surface showed a decreasing trend followed by an increasing trend, while the density of microtexture distribution showed the opposite trend. After a wheel pressure rutting test, the rutted slab showed slight deformation and a certain degree of reduction in 3D structure depth; the deformation of the rutted slab mainly occurred in the surface layer, and the internal deformation was negligible.



**Citation:** Nie, W.; Wang, D.; Yan, J.; Zhang, X. Optimal Design of Mix Proportion of Hot-Mix Epoxy Asphalt Mixture for Steel Bridge Decks and Its Anti-Slip Performance. *Buildings* **2022**, *12*, 437. <https://doi.org/10.3390/buildings12040437>

Academic Editors: Huayang Yu, Xiaopei Cai and Tao Wang

Received: 4 March 2022

Accepted: 30 March 2022

Published: 2 April 2022

**Publisher's Note:** MDPI stays neutral with regard to jurisdictional claims in published maps and institutional affiliations.



**Copyright:** © 2022 by the authors. Licensee MDPI, Basel, Switzerland. This article is an open access article distributed under the terms and conditions of the Creative Commons Attribution (CC BY) license (<https://creativecommons.org/licenses/by/4.0/>).

**Keywords:** road engineering; mix proportion design; slip resistance; friction coefficient; 3D construction depth; microtexture distribution density

## 1. Introduction

Large-span steel bridges are often used as special crossings over special basins, such as the sea, large rivers, or large streams, where traffic volumes are often high [1–4]. Under heavy traffic flow conditions, the anti-slip performance is an indicator that should be a key concern when selecting the type of wear layer and the mix grading design for steel bridge decks [5–8]. Hot-mix epoxy asphalt concrete is widely used on steel bridges with high temperatures and heavy loads, due to its excellent high-temperature stability, low-temperature crack resistance, and ability to follow the deformation of steel plates [9–12]. Epoxy asphalt mix EA-10 is a suspension-dense mix; its coarse aggregate blending ratio is generally about 30%, and the overall gradation is fine. When it is used as an abrasive layer, its surface microstructure is relatively small, and the depth of the structure is generally around 0.2–0.4 mm [13,14]. Under the action of traffic load, the oil film on the surface layer of the EA-10 paving layer will gradually fall off. When the oil film has fallen off to a certain extent, the fine aggregate on the surface layer of the EA-10 gradually falls off, while the coarse aggregate content is relatively small, and under the action of tyre rubbing, the coarse aggregate's corners will gradually be worn off. Therefore, the anti-slip performance of the epoxy asphalt pavement layer shows a change process of first rising and then rapidly falling [15].

The anti-slip performance of asphalt pavements is mainly influenced by vehicle operating characteristics, environment, tyre characteristics, and road surface characteristics,

and the force characteristics are more complex [16–19]. Among the above-mentioned influencing factors, road surface characteristics are the main focus of studies of skid resistance performance on the road. When it comes to surface characteristics, the main factors affecting the skid resistance of asphalt pavements are microtexture, macrotexture, and material properties [20–22]. Material properties include the quality of the raw material, the type of grading, etc., which to a large extent influence the microtexture and macrotexture of asphalt pavements [23–25].

The mechanism of the anti-slip performance of asphalt pavements is the frictional force generated by the mutual coupling between the wearing layer and the tyre. Frictional forces mainly include adhesion, hindrance, and ploughing forces [26,27]—see Figure 1 and Table 1.

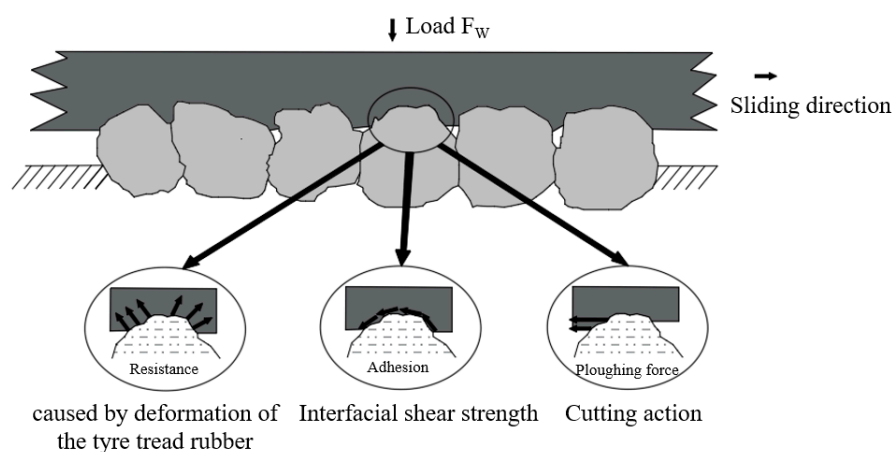


**Figure 1.** Mechanisms of anti-slip performance of asphalt pavements.

**Table 1.** Mechanisms of anti-slip performance of asphalt pavements.

Item	Cause	Influence Factor
Adhesion	Generated by microstructure	Pavement material characteristics, speed of traffic, cleanliness of contact interfaces, etc.
Retention force	Generated by macrostructure	Stone distribution pattern, degree of tyre deformation, etc.
Ploughing force		Stone surface form, tyre rubber hardness, etc.

Research has shown that the design of the asphalt mix proportion is both a very complex scientific problem and an extremely important technical problem. Zhang et al. [28] proposed the use of the CAVF (Coarse Aggregate Void Filling) method to design skeleton-dense asphalt mixes, which can effectively improve the degree of compactness of the mix skeleton. Ge et al. [29] optimized the CVAF method by introducing an interference factor to correct the calculation process and achieve control of the VMA. Based on the previous research, Lu et al. [30] optimized the CAVF method by using the effective asphalt volume instead of the original asphalt aggregate ratio, and the measured coarse skeleton clearance rate instead of the theoretical coarse skeleton clearance rate, which improved the design accuracy. The basic principles of the CAVF method and its improvement methods are mentioned in many papers, so this paper will not repeat them.

Most of the research on hot-mix epoxy asphalt mix EA-10 has been done on the performance of the mix, but less has been done on the slip resistance of the mix [6,31–33]. However, the epoxy asphalt mixture EA-10 has anti-slip performance defects, so improving the anti-slip performance of hot-mix epoxy asphalt mixture to reduce the occurrence of traffic accidents, and to extend the service life of the paving layer, is of great significance [2,34]. In this paper, based on the Nansha Bridge project, the epoxy asphalt mixture was improved, a skeleton-dense epoxy asphalt mixture FAC-10 was proposed as the wear layer for the

steel bridge deck, and the performance of the epoxy asphalt mixture FAC-10 was studied. Meanwhile, based on the actual engineering application, the anti-slip performance of the epoxy asphalt mixture FAC-10 was tracked for a long period using a pavement anti-slip texture tester to study the changes in its anti-slip performance under the action of traffic load, and the effect of traffic load on the deformation of the pavement layer was analyzed by indoor test simulation.

## 2. Materials and Experimental Design

### 2.1. Raw Materials

The raw materials for the pavement layer are shown in Table 2 and the test results of the raw materials are shown in Tables 3–7 and Figure 2. It can be seen from Tables 3–7 that all the test results of the raw materials meet the requirements.

**Table 2.** Raw materials.

Raw Materials	Manufacturers	Remarks
Coarse aggregates	Poly Growth Zhongshan Aggregate Processing Plant: Zhongshan, China	Pyrochlore
Fine aggregates		
Bitumen	Guangzhou Xinyue Asphalt Co., Ltd.: Guangzhou, China	A-70
Epoxy resin	Nippon Kogyo Kasei Co., Ltd.: Fukuoka, Japan	Main agent and curing agent
Mineral powder	Sihui Yuan Tong Building Materials Co., Ltd.: Sihui, China	Limestone

**Table 3.** Coarse aggregate test results.

Test Indicators	Unit	Design Requirements	Test Results	Specifications
Crushing value	%	$\leq 12$	5.5	T 0316
Los Angeles abrasion loss	%	$\leq 16$	10.7	T 0317
Apparent relative density	—	$\geq 2.70$	2.973	T 0304
Water absorption	%	$\leq 1.5$	0.46	T 0304
Firmness	%	$\leq 5$	1.1	T 0314
Pinned particle content	%	$\leq 5$	2.1	T 0312
Water-washed <0.075 mm particle content	%	$\leq 1.0$	0.2	T 0310
Soft stone content	%	$\leq 1$	0.5	T 0320
Polishing value (PSV)	—	$\geq 44$	44	T 0321

**Table 4.** Fine aggregate test results.

Test Indicators	Unit	Design Requirements	Test Results	Specifications
Apparent relative density	—	$\geq 2.70$	2.925	T 0328
Firmness (>0.3 mm fraction)	%	$\leq 5$	1.9	T 0340
Sand equivalent	%	$\geq 70$	80	T 0333
Methylene blue value	g/kg	$\leq 2.5$	0.5	T 0349
Angularity (flow time)	s	$\geq 30$	40.8	T 0345

Table 5. A-70 bitumen test results.

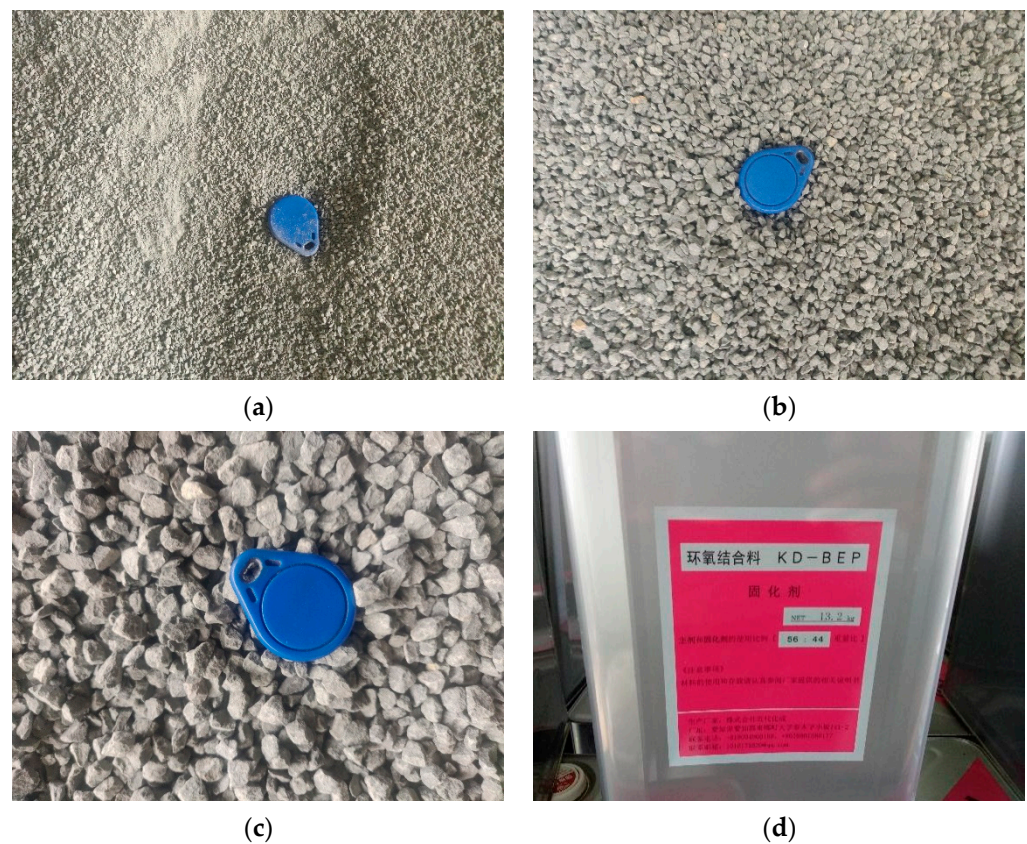
Test Indicators	Unit	Design Requirements	Test Results	Specifications
Needle penetration 25 °C, 100 g, 5 s	0.1 mm	60–80	67	T 0604
Needle penetration index PI	—	−1.5–+1.0	−1.16	T 0604
Softening point $T_{R\&B}$	°C	≥47	47.5	T 0606
Ductility 15 °C, 5 cm/min	cm	≥100	>100	T 0605
Ductility 10 °C, 5 cm/min	cm	≥20	44	T 0605
Density 15 °C	g/cm <sup>3</sup>	≥1.000	1.040	T 0603
Solubility (trichloroethylene)	%	≥99.5	99.8	T 0607
Flash point	°C	≥260	334	T 0611
Wax content	%	≤2.0	1.67	T 0615
Kinetic viscosity 60 °C	Pa·s	≥180	204	T 0620
Film heating for residue testing (163 °C, 5 h)	Quality variation	—	±0.8	T 0610
	Needle penetration ratio: 25 °C	%	≥61	T 0604
	Ductility: 10 °C, 5 cm/min	cm	≥6	T 0605

Table 6. Epoxy resin test results.

Sample Name	Epoxy Resin Main Agent		Specifications
Test Item	Technical Requirements	Test Results	
Viscosity (23 °C, 0.1 pa·s)	1000–5000	2630	T 0625
Flash point (°C)	≥230	239	T 0611
Specific gravity (23 °C)	1.0–1.2	1.15	T 0603
Appearance	Light yellow transparent liquid	Light yellow transparent liquid	—
Name of sample	Epoxy resin curing agent		—
Acid value (mg, KOH/g)	150–200	166	—
Viscosity (23 °C, 0.1 pa·s)	100–800	573	T 0625
Flash point (°C)	≥145	168	T 0611
Specific gravity (23 °C)	0.8–1.0	0.862	T 0603
Appearance	Light yellowish-brown liquid	Light yellowish-brown liquid	—
Name of sample	Epoxy resin bonding compounds		—
Weight ratio (main agent/curing agent)	56/44	56/44	—
Tensile strength (23 °C, MPa)	≥3.0	5.62	GB/T 16777-2008
Elongation at break (23 °C, %)	≥100	297	
Sample name	Epoxy asphalt binding compounds		—
Weight ratio (matrix bitumen/epoxy resin)	50/50	50/50	—
Tensile strength (23 °C, MPa)	≥2.5	3.75	GB/T 16777-2008
Elongation at break (23 °C, %)	≥100	304	

**Table 7.** Mineral powder test results.

Test Indicators	Unit	Design Requirements	Test Results	Specifications
Apparent relative density	—	$\geq 2.50$	2.718	T 0352
Water content	%	$\leq 1$	0.3	T 0103
Appearance	—	No agglomeration	No agglomeration	—
Hydrophilic coefficient	%	$< 1$	0.7	T 0353
Plasticity index	—	$< 4$	3	T 0354
Heating stability	—	Actual measurement records	No significant change	T 0355

**Figure 2.** Raw materials: (a) 0–3 mm aggregate; (b) 3–5 mm aggregate; (c) 5–10 mm aggregate; (d) epoxy resin.

Epoxy asphalt is a kind of thermosetting polymer material. Its thermosetting characteristics are mainly due to the complex formed by the epoxy resin and the curing agent. Epoxy asphalt exists in the form of a 3D cross-linked network structure. This epoxy resin structure forms a continuous phase, and asphalt plays a filling role. The performance of epoxy asphalt is mainly characterized by epoxy resin. The addition ratio of the epoxy resin main agent and the curing agent was 56:44, and the addition ratio of epoxy resin and asphalt was 50:50.

## 2.2. Mixture Preparation

### 2.2.1. Basic Information

#### 1. Pavement layer structure

The steel deck pavement layer of the Nansha Bridge is made of a double-layer epoxy asphalt mix, the structure of which is shown in Figure 3.

Pavement top layer	Epoxy asphalt concrete (coarse gradation), thickness: 35mm
Bonding layer	Epoxy resin binder, quantity: 0.55-0.65mm
Pavement under layer	Epoxy asphalt concrete (coarse graded), thickness: 30mm
Waterproof bonding layer	Epoxy resin binder, dosage: 0.35-0.45mm
Anti-corrosion layer	Epoxy zinc-rich paint: 80-120 $\mu$ m
Steel plate	Sandblasting to remove rust, cleanliness Sa3.0 grade, roughness 80-100 $\mu$ m

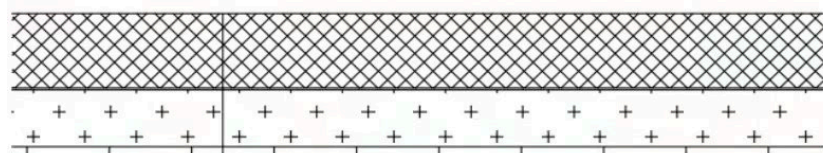


Figure 3. Structural drawing of the steel pavement layer of the steel bridge deck.

## 2. Traffic Volume.

The traffic volumes on the Nansha Bridge since its opening in 2019 are shown in Figure 4, with the majority of traffic (in terms of standard vehicles) ranging from 150,000 to 165,000 vehicles per day, a high proportion of non-minibusses and minivans at 28%, and an average of 20,000 natural vehicles per day in terms of oversized trucks and container trucks.

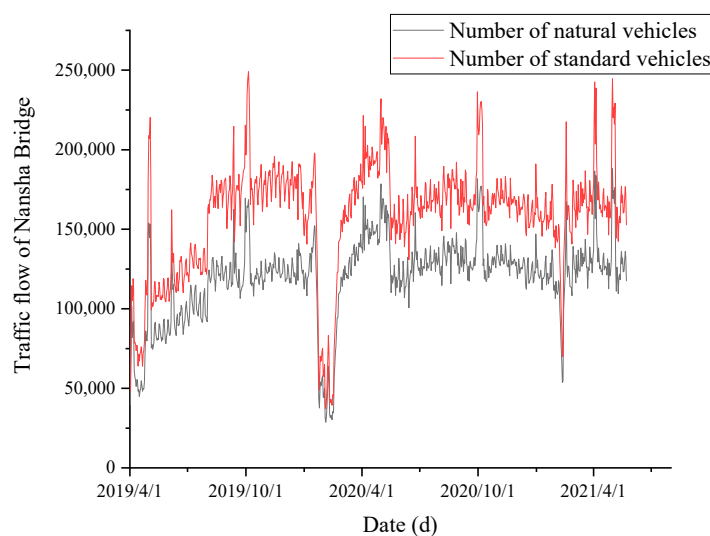


Figure 4. Nansha Bridge traffic volumes.

### 2.2.2. Mix Proportion Design

The wear layer for this project is a skeletal-dense epoxy-rich asphalt mixture FAC (Full Epoxy Asphalt Content) designed by the CAVF method.

The pre-determined mineral powder dosage is 10%, the asphalt aggregate ratio 6.5%, the design void ratio is 2%, the measured tight packing density is 1.888 and the skeleton clearance rate is 36.7%, according to previous experience. The coarse and fine aggregate ratios were calculated to be 69% and 21%, respectively. Combined with the grading requirements, the target mix proportion of FAC-10 was initially determined to be 5–10:3–5:0–3 mm mineral powder (49%:20%:21%:10%) and the asphalt aggregate ratio was 6.5%, in which the ratio of epoxy resin to asphalt was 1:1, and the ratio of epoxy resin host to hardener was 56:44. The synthetic grading is shown in Figure 5, and the ratio verification results are shown in Table 8 [35,36]. As shown in Table 8, the mix proportion was designed according to the mix grading curve calculated by the CAVF method, and the performance of the mixture specimens prepared using the mix proportion design met the design requirements.

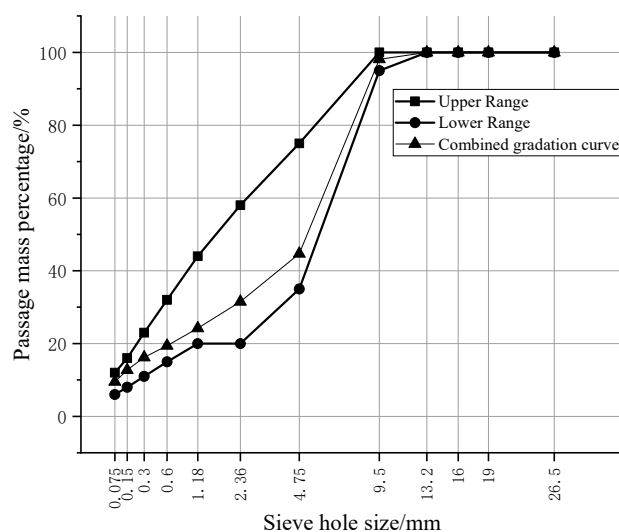


Figure 5. Top pavement FAC-10 grading curve.

Table 8. Mix proportion verification.

Item	Technical Requirements	Result	Specifications
Bulk specific gravity of bituminous mixtures	—	2.565	T 0705
Theoretical maximum specific gravity of bituminous mixtures	—	2.62	T 0705
Void ratio (%)	0–3	2.1	T 0705
Stability (KN)	$\geq 40$	44.89	T 0709
Flow value (mm)	3.0–6.0	5.6	T 0709
Splitting tensile strength ratio (%)	$\geq 90$	91.5	T 0729
Residual stability (%)	$\geq 90$	92.3	T 0709
Dynamic stability at 70 °C (times/mm)	$\geq 10,000$	>10,000	T 0719
Coefficient of water penetration (mL/min)	No water penetration	No water penetration	T 0730
Low-temperature bending	$\geq 3.0 \times 10^{-3}$	$3.58 \times 10^{-3}$	T 0715
Impact toughness (N-mm)	$\geq 3000$	4152	T 0322

### 2.2.3. Steel Deck Pavement

The pavement conditions of the steel bridge deck in different periods are tracked, and the pavement structure in different periods is shown in Figure 6.

## 2.3. Experimental Design

### 2.3.1. Friction Coefficient and Pavement Structure Depth Test

The three indicators, transverse force coefficient, friction coefficient and construction depth, are the indicators used to characterize the anti-slip performance of asphalt pavements in the current specification “Specification for Field Testing of Road Base Pavements” (JTG 3450-2019) [37]. In terms of the form of data collection, the transverse force coefficient is a continuous section test, which is suitable for large area testing in the field, while the friction coefficient and the construction depth are single-point tests, which are suitable for indoor and field testing.

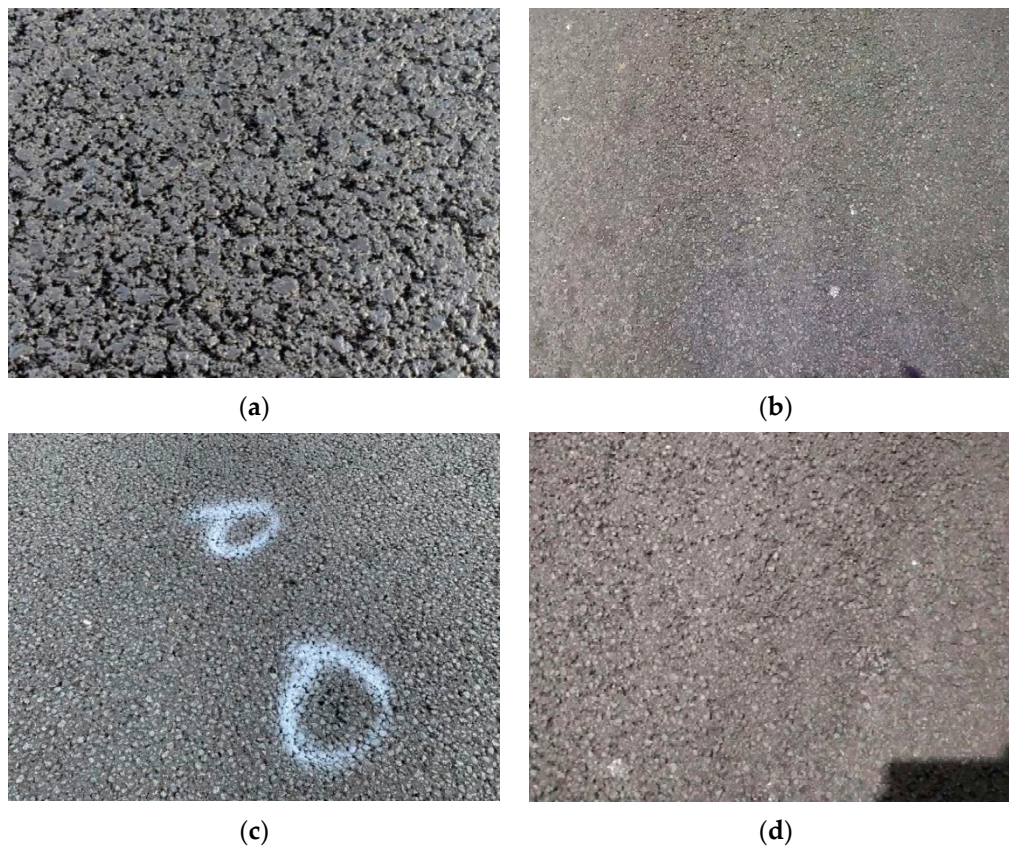


**Figure 6.** Pavement conditions of steel bridge deck during different periods: (a) pavement just after construction; (b) pavement 18 months after opening to traffic; (c) pavement 23 months after opening to traffic; (d) pavement 28 months after opening to traffic.

To investigate the effects of asphalt aggregate ratio on the anti-slip performance of the wear layer, comparative tests were carried out using two mixes, FAC-10 and EA-10, both of which were formed into rutted slabs with asphalt aggregate ratios of 5.9%, 6.2%, 6.5%, 6.8%, and 7.1%. The rutting slabs were subjected to standard conditioning, and then tested for the coefficient of friction and the depth of construction under ambient conditions. The test methods are in line with the Highway Subgrade and Pavement Field Test Specification (JTG T 3450-2019) [37], and the test equipment is shown in Figure 7.

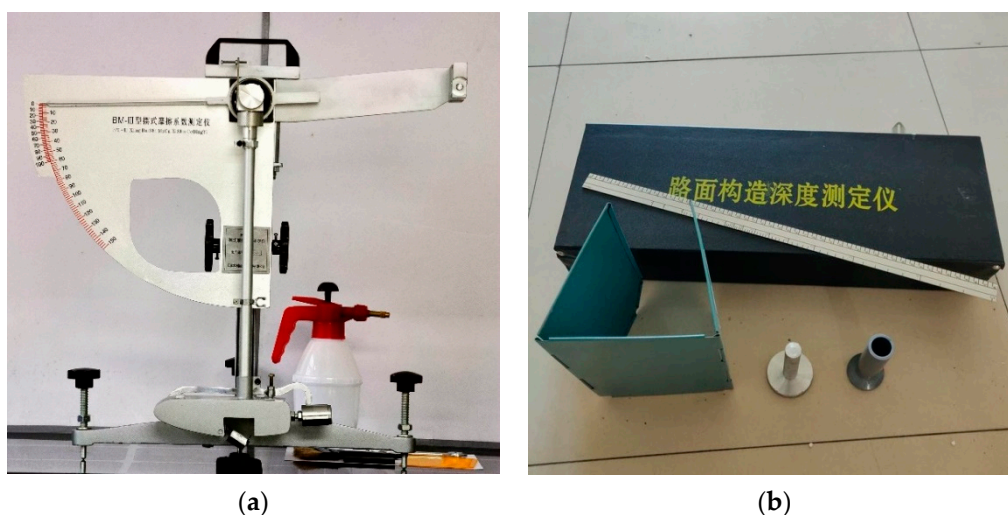


**Figure 7.** Testing equipment: (a) pendulum friction device; (b) pavement structure depth tester.

### 2.3.2. Impact Toughness Test

The asphalt aggregate ratio is not only related to the anti-sliding performance of the wearing course, but also to the anti-fatigue performance of the pavement. To comprehensively consider the durability and skid resistance of the pavement, the impact toughness of the two mixtures under different asphalt aggregate ratios is also tested. The test process is as follows:

- (1) The plate specimens of 300 mm × 300 mm × 50 mm were prepared by a roller compaction molding machine, and the prepared specimens were placed in the oven at 60 °C for 4 days to make them rapidly solidify;
- (2) The solidified specimens were cut into prismatic beams of 250 mm (2 mm) long, 30 mm (0.5 mm) wide, and 35 mm (0.5 mm) high by a high-precision double-sided saw, and the span was 200 mm (0.5 mm), as shown in Figure 8;
- (3) We put the cut specimens into the environmental incubator for more than 4 h at 15 °C. After heat preservation, we performed an impact toughness test, as shown in Figure 9. The impact toughness test is carried out on the MTS testing machine. The loading rate of the testing machine can be adjusted according to the needs. The loading rate of this test was 500 mm/min.



**Figure 8.** Specimen fabrication: (a) formed rut plate; (b) cutting beam.



**Figure 9.** Impact toughness test.

### 2.3.3. Surface Anti-Slip Tracking Test

To investigate in depth the changes in the anti-slip performance of FAC-10 during the functioning of the real bridge, a pavement anti-slip texture tester was used to test the anti-slip performance of the pavement. The pavement anti-skid texture tester was developed by the Guangzhou Xiaoning Institute of Roadway Engineering. The test system consists of a

laser sensor, an electrical control system, a data acquisition system, data processing, and a display system [38]. The equipment parameters of the pavement anti-skid texture tester are based on previous research, as shown in Table 9 [39].

**Table 9.** The parameters of the pavement anti-slip texture tester.

Item	Parameter
Effective range of elevation measurement	$\pm 23$ mm
Measurement accuracy	$\leq 0.01$ mm
Dot resolution	0.05 mm
Laser beamline width	25–39 mm
Maximum measuring range	$300 \times 300$ mm
Data acquisition speed	$\leq 0.64$ m/s
Texture elevation calibration error	$< 0.1\%$
System operating environment	Temperature 0–45 °C; relative humidity 20–85% (non-condensing)

The pavement anti-slip texture tester and its principle are shown in Figure 10. The calculation formula is Equation (1):

$$PS = \frac{count - (2^{16}/2)}{2^{16}/2} \times 2 \times sf \times 10^{-dp} \quad (1)$$

where  $PS$  is the elevation;  $count$  is the laser device measurement;  $sf$  is the amplification factor;  $dp$  is the laser device point position factor.

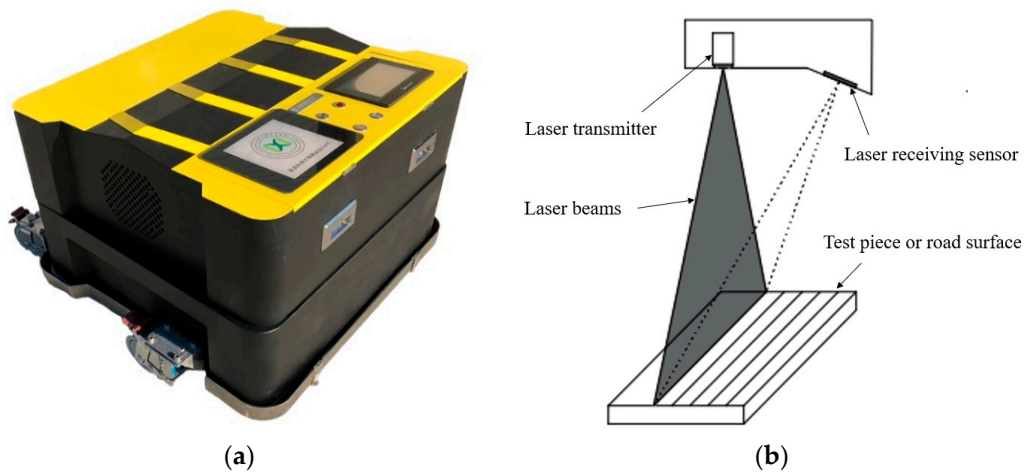


**Figure 10.** The anti-slip texture tester and the principle of the pavement: (a) anti-slip texture tester for road surfaces; (b) principle of the road surface anti-slip texture tester.

The scanning area of the road surface texture tester was set to  $180 \times 180$  mm, and the test results output the 3D construction depth and microtexture distribution density of the area.

The ratio of the approximate volume of the structural envelope of the 3D surface of the road to the horizontal projected area of the 3D surface is the 3D structural depth, and the formula is Equation (2).

$$S_{TD} = \frac{V}{A} = \frac{I_1 + 2 \sum_{i=2}^{n-1} I_i d + I_n}{2(n-1)d} \times l \quad (2)$$

where  $S_{TD}$  is the average construction depth of the three-dimensional surface of the road, mm;  $V$  is the approximate volume of the construction envelope of the three-dimensional surface of the road;  $A$  is the horizontal projection area of the three-dimensional surface;  $I_1$  is the average section depth under the two-dimensional contour of the road table;  $I_i$  is the average section depth of the  $i$  contour line, mm;  $n$  is the number of contour lines;  $d$  is the contour line collection spacing in the  $Y$  direction, mm;  $l$  is the length of the contour curve, mm.

The microscopic texture distribution density is the texture area per unit reference plane, and is used to characterize the degree of density of the road surface configuration distribution, which is calculated as Equation (3).

$$S_{MI} = \frac{A_T}{a \times b} \quad (3)$$

where  $S_{MI}$  is the density of the microscopic texture distribution;  $A_T$  is the area of the microscopic 3D surface, mm<sup>2</sup>;  $a, b$  is the side length of the measurement area, mm.

#### 2.3.4. Rutting Test + 3D Construction Depth Test

The epoxy asphalt mix is a thermosetting material, and it is assumed that the paving layer will not deform again after it has been fully cured and developed strength [40]. To further investigate the effect of traffic load on the paving layer, the rutting test was carried out on a rutting slab, and the change in the three-dimensional construction depth before and after the rutting test was examined. Three rutting slabs were formed following the above target ratio, and the rutting slabs were allowed to develop for 4 days under standard maintenance conditions at  $60 \pm 1$  °C. After the 4 days of development, the slabs were left at room temperature for 1 day and scanned for 3D construction depth using a pavement skid resistance texture tester, and then rutting tests were carried out according to the test method dictated by “Standard Test Methods of Bitumen and Bituminous Mixtures for Highway Engineering” (JTG E20-2011) [37]. After the rutting test, the rutting slabs were left at room temperature for 1 day and then scanned for 3D construction depth. The test process is shown in Figure 11.



**Figure 11.** Road surface sliding resistance test: (a) test direction; (b) total rutting slab deformation.

### 3. Results and Discussion

#### 3.1. Effect of Asphalt Aggregate Ratio on Anti-Slip Properties

The results of friction coefficient and pavement structure depth test are shown in Figures 12 and 13. As can be seen from the figures, the higher the asphalt aggregate ratio, the smaller the friction coefficient and depth of construction, and the poorer the anti-slip performance. This trend, whereby smaller values of TD and BPN reflect worse skid resistance, is consistent with the findings of previous studies [41]. When the asphalt aggregate ratio is less than 6.9%, the friction coefficient values of FAC-10 and EA-10 do

not differ much under the same conditions of asphalt aggregate ratio. When the asphalt aggregate ratio is greater than 6.9%, the surface of EA-10 is heavily oiled, and the coefficient of friction drops more significantly. Under the same conditions of asphalt aggregate ratio, the tectonic depth of FAC-10 is significantly greater than that of EA-10. Under the same conditions of asphalt aggregate ratio, the construction depth of FAC-10 is significantly greater than that of EA-10. Combining the friction coefficient and construction depth index, the anti-slip performance of FAC-10 is better than that of EA-10.

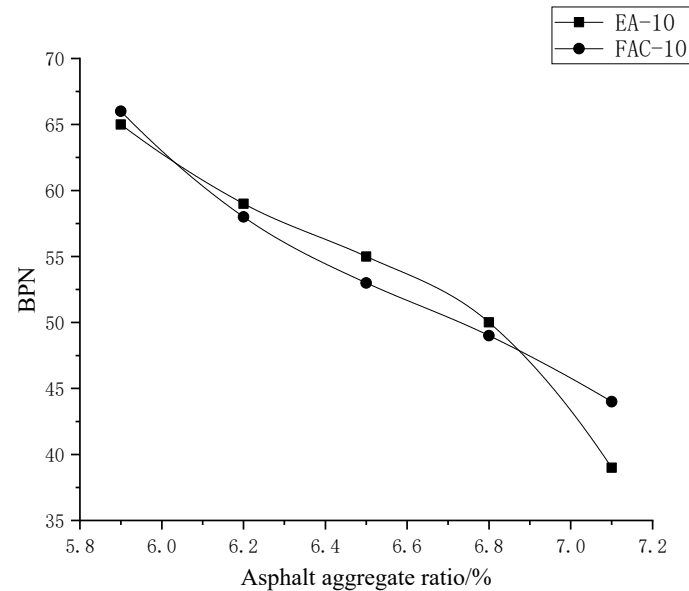


**Figure 12.** A plot of different asphalt aggregate ratio versus friction coefficient.

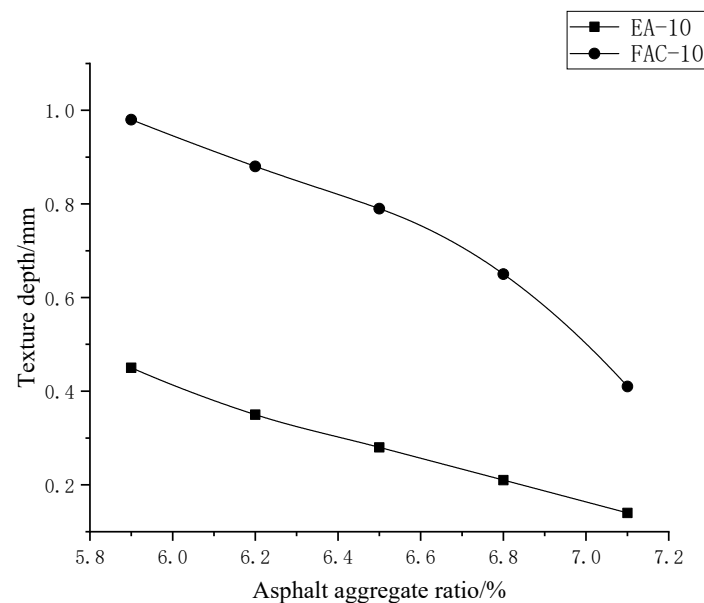


**Figure 13.** A plot of different asphalt aggregate ratio versus tectonic depth.

### 3.2. Effect of Asphalt Aggregate Ratio on Fatigue Resistance

The results of the impact toughness test for the two mixtures with different asphalt aggregate ratios are shown in Figure 14. It can be seen from Figure 14 that the fatigue resistance of EA-10 is slightly better than that of FAC-10. The impact toughness increases with the increase in asphalt content. When the asphalt aggregate ratio increases to 6.5%, the impact toughness of the asphalt aggregate ratio decreases gradually. Therefore, the threshold points of EA-10 and FAC-10 are 6.5%.

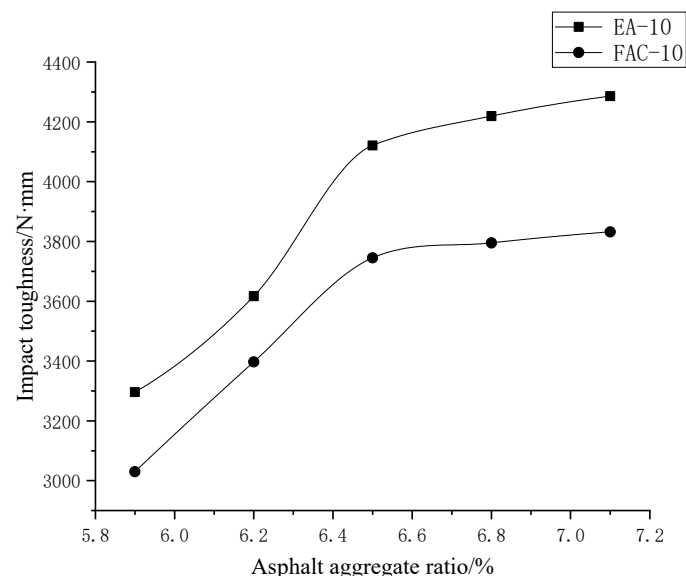


**Figure 14.** Relationship between different asphalt aggregate ratios and impact toughness.

In summary, out of the two epoxy asphalt mixes EA-10 and FAC-10, the epoxy asphalt mix EA-10 has better fatigue resistance and is more suitable for application in the lower layer of the pavement, while epoxy asphalt mix FAC-10 has better anti-slip properties and is more suitable for use as the upper layer of the steel bridge deck pavement.

### 3.3. Surface Anti-Slip Texture Analysis of Abrasion Layer FAC-10

The anti-slip performance of the Nansha Bridge paving layer FAC-10 was tracked and tested at four points in April 2019 (before opening to traffic), October 2020, March 2021, and August 2021. The test location was the left lane wheel track zone, with 14 test points taken at the same location for each test. The 3D structural depth detection is shown in Figure 15, and the results of the 3D structure depth and microtexture distribution density are shown in Figures 16 and 17. As can be seen from Figure 16, the 3D structure depth of the road surface tended to decrease during the first 18 months after the opening of the bridge, while the 3D structure depth of the road surface tended to increase between 18 and 28 months after the opening of the bridge. As can be seen from Figure 17, the microtexture distribution density of the road surface showed an increasing trend in the first 23 months after opening, and a decreasing trend between 23 and 28 months after opening. The microtexture distribution density mainly provides the adhesion component of tyre friction. When epoxy asphalt mix construction is complete, the surface of the aggregate will be attached to a thick layer of asphalt film. In the asphalt film and tyre contact process, the asphalt film will gradually wear, and the aggregate itself will also gradually reveal its micro-texture. This is consistent with the findings of previous studies, wherein the skid resistance evolves continuously under traffic polishing, with the traffic first removing the initial binder film and then progressively polishing the microtexture of the aggregates [42]. After some time, the density of the microtexture distribution of the surface layer will gradually increase. When the asphalt film is worn more severely, the microtexture of the aggregate will also be worn by the tyres, at which point there will be a decrease in the density of the microtexture distribution.

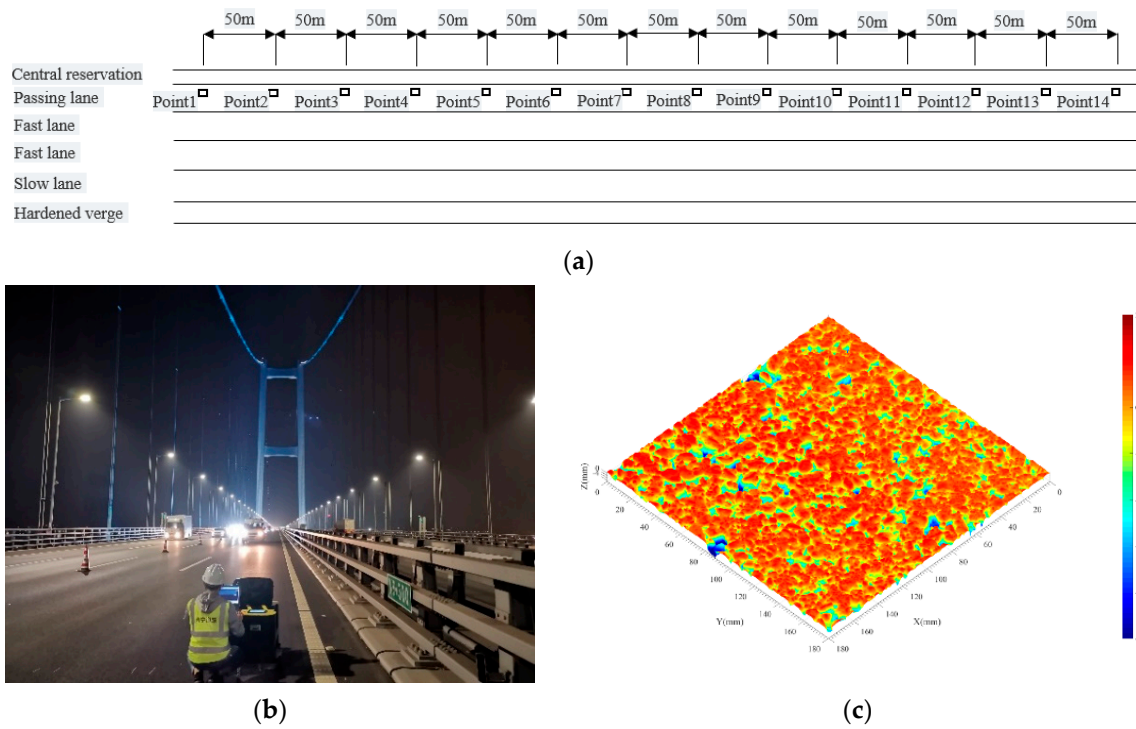


Figure 15. Three-dimensional structural depth detection: (a) detection position; (b) field test; (c) microscopic cloud map of the road surface.

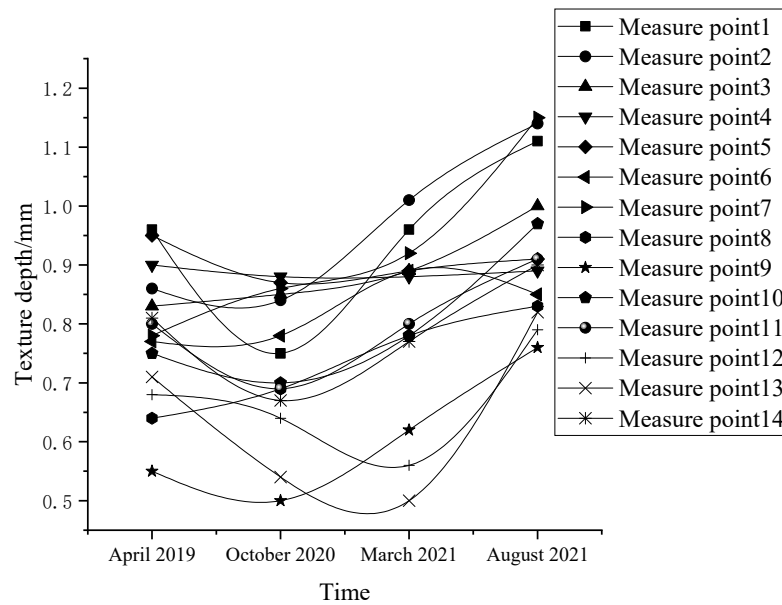


Figure 16. Results of the 3D construction depth inspection.

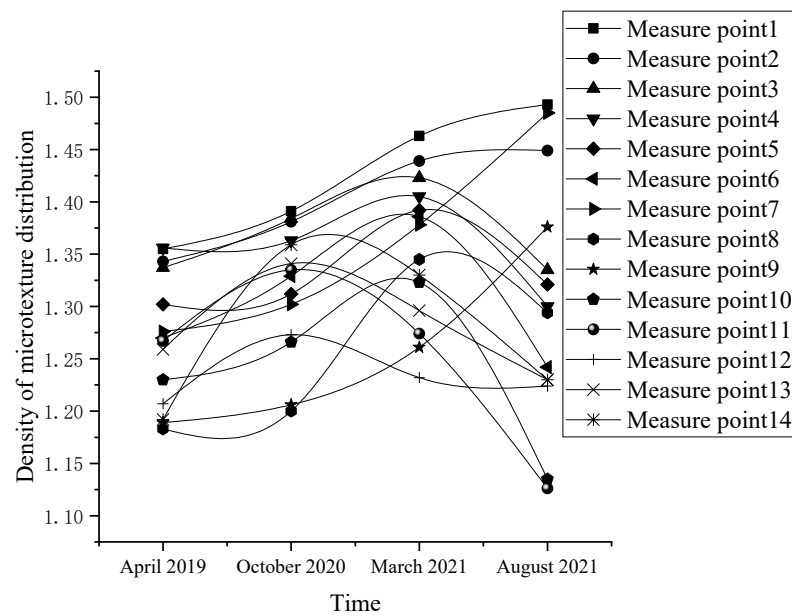


Figure 17. Microtexture distribution density detection results.

### 3.4. Anti-Slip Performance Analysis of Abrasive Layer FAC-10

The results of the rutting test are shown in Table 10. As can be seen from Table 10, a slight deformation of the rutting slab occurred after the wheel press was applied. The 3D depth of construction also decreased to a certain extent. From the 3D depth of construction and the total deformation values, we can see that the deformation of the rutting slab occurred mainly in the surface layer, while the internal deformation was negligible. Although the epoxy bitumen mix is a thermosetting material, slight deformation in the surface layer of the aggregate occurred under the action of the traffic load, which is consistent with previous findings [6,43]. Therefore, the proposed mixture FAC-10 could meet the operating requirements of a steel bridge pavement, and dramatically improve the skid-resistance of an epoxy asphalt concrete pavement.

Table 10. Rutting test results.

SN.	Pre-Test 3D Construction Depth/mm	Total Rutting Slab Deformation/mm	Post-Test 3D Construction Depth/mm
1	0.96	0.212	0.76
2	0.86	0.185	0.69
3	0.81	0.181	0.65

Note: The total rutting slab deformation of the rut plate is the vertical displacement of the rut plate.

## 4. Conclusions

In this paper, a new type of steel bridge deck pavement is proposed with consideration of the design principle of a rich asphalt mix proportion, and through comparison tests with traditional epoxy asphalt mixed, it is verified that the new epoxy asphalt mix is more suitable than the upper layer of steel bridge deck pavements. The change process of the anti-slip performance of the new paving material was studied through 2.5 years of anti-slip performance tracking, and the effect of the traffic load on the anti-slip performance of the paving layer material was analyzed through indoor test simulation. The conclusions are as follows:

- The higher the asphalt aggregate ratio, the smaller the friction coefficient and depth of construction. When the asphalt aggregate ratio is less than 6.9%, the friction coefficient values of FAC-10 and EA-10 do not differ much under the same conditions of asphalt

aggregate ratio. When the asphalt aggregate ratio is greater than 6.9%, the surface of EA-10 is heavily oiled, and the coefficient of friction decreases more significantly. Under the same conditions of asphalt aggregate ratio, the tectonic depth of FAC-10 is significantly greater than that of EA-10. Under the same conditions of asphalt aggregate ratio, the construction depth of FAC-10 is significantly greater than that of EA-10. The combined friction coefficient and construction depth indexes show that the anti-slip performance of FAC-10 is better than that of EA-10;

- The results of the pavement anti-slip texture tester show that the depth of the 3D structure of the road surface tends to decrease and then increase during the monitoring period, while the density of the microtexture distribution shows the opposite trend;
- From the results of the rutting tests, we see that the rutting slab showed slight deformation and a certain degree of reduction in its 3D construction depth after wheel pressure was applied, the deformation of the rutting slab mainly occurred in the surface layer, and the internal deformation was negligible.
- In follow-up studies, the steel bridge deck pavement structure can be studied by the finite element numerical simulation method to study the changes in pavement structure under different testing conditions.

**Author Contributions:** Conceptualization, W.N. and D.W.; methodology, W.N. and D.W.; software, J.Y.; validation, W.N. and D.W.; formal analysis, W.N.; investigation, J.Y.; resources, X.Z.; data curation, W.N.; writing—original draft preparation, W.N.; writing—review and editing, W.N.; supervision, D.W.; project administration, D.W.; funding acquisition, D.W. All authors have read and agreed to the published version of the manuscript.

**Funding:** This research was funded by the Natural Science Fund of Guangdong Province, grant number 2019A1515011965, and Natural Science Foundation of China, grant number 51808228.

**Institutional Review Board Statement:** Not applicable.

**Informed Consent Statement:** Not applicable.

**Data Availability Statement:** The data presented in this study are available on request from the corresponding author.

**Conflicts of Interest:** The authors declare no conflict of interest.

## References

1. Qin, S.; Gao, Z. Developments and Prospects of Long-Span High-Speed Railway Bridge Technologies in China. *Engineering* **2017**, *3*, 787–794. [[CrossRef](#)]
2. Wang, Z.; Zhang, S. Fatigue endurance limit of epoxy asphalt concrete pavement on the deck of long-span steel bridge. *Int. J. Pavement Res. Technol.* **2018**, *11*, 408–415. [[CrossRef](#)]
3. Yang, Y.; Fahmy, M.F.M.; Guan, S.; Pan, Z.; Zhan, Y.; Zhao, T. Properties and applications of FRP cable on long-span cable-supported bridges: A review. *Compos. Part B Eng.* **2020**, *190*, 107934. [[CrossRef](#)]
4. Chen, L.; Liu, G.; Zhang, X.; Pan, G. An innovative interface reinforcement method for steel bridge deck pavement pothole repair. *Constr. Build. Mater.* **2021**, *298*, 123838. [[CrossRef](#)]
5. Zhang, M.; Hao, P.; Men, G.; Liu, N.; Yuan, G. Research on the compatibility of waterproof layer materials and asphalt mixture for steel bridge deck. *Constr. Build. Mater.* **2021**, *269*, 121346. [[CrossRef](#)]
6. Qian, Z.-d.; Liu, Y.; Liu, C.-b.; Zheng, D. Design and skid resistance evaluation of skeleton-dense epoxy asphalt mixture for steel bridge deck pavement. *Constr. Build. Mater.* **2016**, *114*, 851–863. [[CrossRef](#)]
7. Liu, C.; Qian, Z.; Liao, Y.; Ren, H. A Comprehensive Life-Cycle Cost Analysis Approach Developed for Steel Bridge Deck Pavement Schemes. *Coatings* **2021**, *11*, 565. [[CrossRef](#)]
8. Chehelgo, K.; C. Abiero Gariy, Z.; Muse Shitote, S. Laboratory Mix Design of Cold Bitumen Emulsion Mixtures Incorporating Reclaimed Asphalt and Virgin Aggregates. *Buildings* **2018**, *8*, 177. [[CrossRef](#)]
9. Cong, P.; Luo, W.; Xu, P.; Zhang, Y. Chemical and physical properties of hot mixing epoxy asphalt binders. *Constr. Build. Mater.* **2019**, *198*, 1–9. [[CrossRef](#)]
10. Peng, C.; Hu, X.; You, Z.; Xu, F.; Jiang, G.; Ouyang, H.; Guo, C.; Ma, H.; Lu, L.; Dai, J. Investigation of anti-icing, anti-skid, and water impermeability performances of an acrylic superhydrophobic coating on asphalt pavement. *Constr. Build. Mater.* **2020**, *264*, 120702. [[CrossRef](#)]

11. Xie, H.; Li, C.; Wang, Q. A critical review on performance and phase separation of thermosetting epoxy asphalt binders and bond coats. *Constr. Build. Mater.* **2022**, *326*, 126792. [[CrossRef](#)]
12. Yu, H.; Leng, Z.; Zhang, Z.; Li, D.; Zhang, J. Selective absorption of swelling rubber in hot and warm asphalt binder fractions. *Constr. Build. Mater.* **2020**, *238*, 117727. [[CrossRef](#)]
13. Nie, W.; Wang, D.; Sun, Y.; Xu, W.; Xiao, X. Integrated Design of Structure and Material of Epoxy Asphalt Mixture Used in Steel Bridge Deck Pavement. *Buildings* **2022**, *12*, 9. [[CrossRef](#)]
14. Li, Y.; Cao, D.; Zhang, Y.; Jia, X. Performance of a dry-method-epoxy modifier and a modified epoxy-asphalt mixture. *Constr. Build. Mater.* **2021**, *266*, 120229. [[CrossRef](#)]
15. Zhong, K.; Yang, X.; Wei, X. Investigation on surface characteristics of epoxy asphalt concrete pavement. *Int. J. Pavement Res. Technol.* **2017**, *10*, 545–552. [[CrossRef](#)]
16. Guo, F.; Pei, J.; Zhang, J.; Li, R.; Zhou, B.; Chen, Z. Study on the skid resistance of asphalt pavement: A state-of-the-art review and future perspective. *Constr. Build. Mater.* **2021**, *303*, 124411. [[CrossRef](#)]
17. Yu, M.; You, Z.; Wu, G.; Kong, L.; Liu, C.; Gao, J. Measurement and modeling of skid resistance of asphalt pavement: A review. *Constr. Build. Mater.* **2020**, *260*, 119878. [[CrossRef](#)]
18. Huang, X.; Zheng, B. Research Status and Progress for Skid Resistance Performance of Asphalt Pavements. *China J. Highw. Transp.* **2019**, *32*, 32–49.
19. Yu, H.; Zhu, Z.; Leng, Z.; Wu, C.; Zhang, Z.; Wang, D.; Oeser, M. Effect of mixing sequence on asphalt mixtures containing waste tire rubber and warm mix surfactants. *J. Clean. Prod.* **2020**, *246*, 119008. [[CrossRef](#)]
20. Zhang, X.; Chen, E.; Li, N.; Wang, L.; Si, C.; Wang, C. Micromechanical analysis of the rutting evolution of asphalt pavement under temperature–stress coupling based on the discrete element method. *Constr. Build. Mater.* **2022**, *325*, 126800. [[CrossRef](#)]
21. Yin, Y.; Han, S.; Kong, H.; Han, X.; Guo, H. Optimization and performance evaluation of waterborne epoxy resin modified emulsified asphalt micro-surfacing based on tunnel driving environment. *Constr. Build. Mater.* **2022**, *315*, 125604. [[CrossRef](#)]
22. Zhang, S.; Wang, D.; Guo, F.; Deng, Y.; Feng, F.; Wu, Q.; Chen, Z.; Li, Y. Properties investigation of the SBS modified asphalt with a compound warm mix asphalt (WMA) fashion using the chemical additive and foaming procedure. *J. Clean. Prod.* **2021**, *319*, 128789. [[CrossRef](#)]
23. Yu, H.; Leng, Z.; Zhou, Z.; Shih, K.; Xiao, F.; Gao, Z. Optimization of preparation procedure of liquid warm mix additive modified asphalt rubber. *J. Clean. Prod.* **2017**, *141*, 336–345. [[CrossRef](#)]
24. Yu, H.; Leng, Z.; Dong, Z.; Tan, Z.; Guo, F.; Yan, J. Workability and mechanical property characterization of asphalt rubber mixtures modified with various warm mix asphalt additives. *Constr. Build. Mater.* **2018**, *175*, 392–401. [[CrossRef](#)]
25. Yu, H.; Deng, G.; Zhang, Z.; Zhu, M.; Gong, M.; Oeser, M. Workability of rubberized asphalt from a perspective of particle effect. *Transp. Res. Part D Transp. Environ.* **2021**, *91*, 102712. [[CrossRef](#)]
26. Yu, J.; Zhang, B.; Long, P.; Chen, B.; Guo, F. Optimizing the Texturing Parameters of Concrete Pavement by Balancing Skid-Resistance Performance and Driving Stability. *Materials* **2021**, *14*, 6137. [[CrossRef](#)] [[PubMed](#)]
27. Zhang, S. Research on Multi-scale Asphalt Pavement SkidResistance Based on Interface Contact Performance. Ph.D. Thesis, South China University of Technology, Guangzhou, China, 2015.
28. Zhang, X.; Wang, S.; Wu, K.; Wang, D. CAVF method for asphalt mix composition design. *Highway* **2001**, *12*, 5.
29. Ge, Z.; Zhang, X.; Gao, J. Improvement of design method of rich asphalt mixture. *J. Highw. Transp. Res. Dev.* **2007**, *24*, 48–50.
30. Lu, X. Research on Aggregate Gradation Optimum and MixtureDesign Methods of OGFC in Guangdong Region. Master’s Thesis, South China University of Technology, Guangzhou, China, 2015.
31. Liu, Y.; Qian, Z.; Shi, X.; Zhang, Y.; Ren, H. Developing cold-mixed epoxy resin-based ultra-thin antiskid surface layer for steel bridge deck pavement. *Constr. Build. Mater.* **2021**, *291*, 123366. [[CrossRef](#)]
32. Zhang, H.; Mao, Q.; Zhu, Z.; Zhang, Z.; Pan, Y.; Wan, J.; Zhou, C.; Qian, J. Experimental study on service performance of epoxy asphalt steel deck pavement of cable stayed bridge. *Case Stud. Constr. Mater.* **2020**, *13*, e00392. [[CrossRef](#)]
33. He, Q.; Zhang, H.; Li, J.; Duan, H. Performance evaluation of polyurethane/epoxy resin modified asphalt as adhesive layer material for steel-UHPC composite bridge deck pavements. *Constr. Build. Mater.* **2021**, *291*, 123364. [[CrossRef](#)]
34. Konečný, P.; Lehner, P. Durability assessment of concrete bridge deck considering waterproof membrane and epoxy-coated reinforcement. *Perspect. Sci.* **2016**, *7*, 222–227. [[CrossRef](#)]
35. Hoang, V.H.; Nguyen, Q.T.; Tran, A.T.; Tran, T.C.H.; Do, T.A. Mechanical behavior of the asphalt wearing surface on an orthotropic steel bridge deck under cyclic loading. *Case Stud. Constr. Mater.* **2022**, *16*, e00836. [[CrossRef](#)]
36. Xu, W.; Wei, X.; Wei, J.; Chen, Z. Experimental Evaluation of the Influence of Aggregate Strength on the Flexural Cracking Behavior of Epoxy Asphalt Mixtures. *Materials* **2020**, *13*, 1876. [[CrossRef](#)]
37. *JTG 3450-2019-2011*; Field Test Methods of Highway Subgrade and Pavement. Ministry of Transport of the People’s Republic of China: Beijing, China, 2011.
38. Li, W.; Zhang, X.; Chen, B.; Yu, J.; Li, Z. Evaluation on Asphalt Pavement Skid Resistance Based on Contact Stress Concentration. *Sci. Technol. Eng.* **2018**, *18*, 107–113. [[CrossRef](#)]
39. Chen, B. Research on Asphalt Pavement Skid Resistance Performance Evaluation Method Based on Tire-Pavement Effective Contact Characteristics. Ph.D Thesis, South China University of Technology, Guangzhou, China, 2018.
40. Xu, W.; Wei, J.; Chen, Z.; Wang, F.; Zhao, J. Evaluation of the Effects of Filler Fineness on the Properties of an Epoxy Asphalt Mixture. *Materials* **2021**, *14*, 2003. [[CrossRef](#)] [[PubMed](#)]

41. Li, J.; Zhang, Q.; Chen, Z. Skid resistance decay model of epoxy wear layer on cement pavement. *J. Shenzhen Univ. (Sci. Eng.)* **2017**, *34*, 597–603. [[CrossRef](#)]
42. Kane, M.; Edmondson, V. Modelling the bitumen scour effect: Enhancement of a dynamic friction model to predict the skid resistance of rubber upon asphalt pavement surfaces subjected to wear by traffic polishing. *Wear* **2018**, *400–401*, 100–110. [[CrossRef](#)]
43. Xiang, Q.; Xiao, F. Applications of epoxy materials in pavement engineering. *Constr. Build. Mater.* **2020**, *235*, 117529. [[CrossRef](#)]